

TRAJECTORY SELECTION STRATEGY FOR TOURS IN THE EARTH-MOON SYSTEM

**Amanda F. Haapala^{*}, Mar Vaquero[†], Thomas A. Pavlak[‡],
Kathleen C. Howell[‡], and David C. Folta[§]**

As mission requirements become increasingly complex, improved flexibility in mission design tools is vital. Strategies that offer interactive access to a variety of solutions supply an enhanced perspective of the design space. In this investigation, interactive and automated trajectory design tools are examined for applications in the Earth-Moon system. Operating within a graphical user interface, these tools offer a composite view of multi-body orbits possessing a variety of characteristics, and facilitate the assembly of end-to-end mission designs via interactive selection of trajectory arcs with desirable characteristics. Final designs are imported into NASA's General Mission Analysis Tool for validation and further access in a mission setting.

INTRODUCTION

Improved flexibility in trajectory design tools is essential to accommodate increasing complexity in mission requirements. Strategies that offer interactive access to a variety of solutions provide an enhanced perspective of the design space, and enable the rapid design and analysis of trajectory options. Several tools exist that exploit dynamical systems theory for mission design, including Generator^{1,2} and LTool.³ A tool to interactively compute libration point orbits and their associated manifolds is demonstrated by Mondelo et al.⁴ The software AUTO allows for computation of periodic orbits, numerical continuation of orbit families, and bifurcation detection and analysis.⁵ Additionally, an interactive design approach based in visual analytics has been previously demonstrated by Schlei for a variety of mission design applications in multi-body regimes.⁶ In this investigation, an Adaptive Trajectory Design (ATD) strategy, providing access to a composite view of multi-body orbits possessing a variety of characteristics within one interactive design setting, is demonstrated. The availability of a large assortment of orbit types within one mission design environment offers the user a unique perspective in which various mission design options may be explored, and the effectiveness of different orbits in meeting mission requirements may be evaluated. In this analysis, trajectory designs that incorporate theoretical solutions from the Circular Restricted Three-Body (CR3B) model are demonstrated in the Earth-Moon system using the interactive ATD environment, in which trajectories are assembled via point-and-click arc selection. Once a discontinuous baseline is assembled within the design environment, it is then transitioned into a unified higher-fidelity

^{*}Ph.D. Candidate, Purdue University, School of Aeronautics and Astronautics, West Lafayette, Indiana 47907.

[†]Ph.D. Candidate, Purdue University, School of Aeronautics and Astronautics, West Lafayette, Indiana 47907; currently, Jet Propulsion Laboratory, Pasadena, California 91109

[‡]Hsu Lo Distinguished Professor of Aeronautics and Astronautics, Purdue University, School of Aeronautics and Astronautics, West Lafayette, Indiana 47907. Fellow AAS; Fellow AIAA.

[§]Aerospace Engineer, NASA Goddard Space Flight Center, Greenbelt, Maryland 20771.

ephemeris model via interactive ATD differential corrections environments. The final trajectory is imported into NASA's General Mission Analysis Tool (GMAT)^{7,8} where it can be accessed in a mission setting for further analysis.

An interactive design environment that supplies a composite view of multi-body orbits is not only useful from a trajectory design perspective, but also to gain insight into the relationships between different orbit types. For example, the role of invariant manifolds in facilitating the resonance transitions experienced by several Jupiter-family comets has been examined by previous researchers, e.g., Koon et al.⁹ The relationship between Distant Prograde Orbits (DPOs)¹⁰ and libration point orbits has been demonstrated by Parker et al.¹¹ The transfer trajectories for the P1 and P2 spacecraft from the ARTEMIS¹² mission incorporate stable and unstable manifolds associated with libration point orbits in the vicinity of L_1 and L_2 ; a merged view of the P1 and P2 mission orbits with members from the family of DPOs in the Earth-Moon system reveals an association between these orbit structures. In this composite view, it is apparent that the transfers employed for ARTEMIS inherit characteristics associated with nearby DPOs. Orbits from the family of DPOs near the energy level associated with the ARTEMIS trajectories are unstable, and, therefore, possess stable and unstable manifolds that asymptotically approach and depart the orbits. Exploiting these manifold structures, heteroclinic connections^{9,11} (free transfers) are computed that closely resemble the transfers executed by the ARTEMIS spacecraft.

CIRCULAR RESTRICTED THREE-BODY MODEL

The CR3B model¹³ proves useful for preliminary analysis of trajectory options within the Earth-Moon system. The motion of a spacecraft, assumed massless, is determined by the gravitational forces of the Earth and the Moon, each represented as a point mass. The orbits of the Earth and Moon are assumed to be circular relative to the system barycenter. A barycentric rotating frame is defined such that the rotating x -axis is directed from the Earth to the Moon, the z -axis is parallel to the direction of the angular velocity of the primary system, and the y -axis completes the right-handed, orthonormal triad. The position of the spacecraft relative to the Earth-Moon barycenter is defined in terms of rotating coordinates as $\mathbf{r} = [x, y, z]$, where bold symbols denote vector quantities. The mass parameter is defined as $\mu = \frac{m_2}{m_1 + m_2}$, where m_1 and m_2 correspond to the mass of the Earth and Moon, respectively. The first-order, nondimensional, vector equation of motion is

$$\dot{\mathbf{x}} = \mathbf{f}(\mathbf{x}), \quad (1)$$

where the vector field, $\mathbf{f}(\mathbf{x})$, is defined

$$\mathbf{f}(\mathbf{x}) = [\dot{x}, \dot{y}, \dot{z}, 2n\dot{y} + U_x, -2n\dot{x} + U_y, U_z], \quad (2)$$

noting that the nondimensional mean motion of the primary system is $n = 1$. In Equation (2), $U(x, y, z, n) = \frac{1-\mu}{d} + \frac{\mu}{r} + \frac{1}{2}n^2(x^2 + y^2)$ is the pseudo-potential function, with the nondimensional Earth-spacecraft and Moon-spacecraft distances written as d and r , respectively, and the quantities U_x, U_y, U_z represent partial derivatives of U with respect to rotating position coordinates. The only known integral of the motion is the Jacobi constant, evaluated as $C = 2U - v^2$, where $v = (\dot{x}^2 + \dot{y}^2 + \dot{z}^2)^{1/2}$. This quantity is a constant of motion in the rotating frame and provides useful information about the energy level associated with a given solution in the CR3B model.

ADAPTIVE TRAJECTORY DESIGN STRATEGIES

In response to an increasing need for a fast and efficient trajectory design process that utilizes well known multi-body solutions, an effort was initiated to develop an interactive design environment.* An interactive design strategy that incorporates a variety of theoretical solutions (e.g., conic arcs, periodic and quasi-periodic libration point orbits, invariant manifolds, P_1 - and P_2 -centered orbits in the CR3B model, etc.) offers an environment in which exploration of the design space is simple and efficient. Rather than locating single point solutions, a more thorough search of the global solution space is facilitated. In this investigation, Adaptive Trajectory Design (ATD) strategies that supply access to a composite view of multi-body orbits possessing a variety of characteristics are examined. Using graphical user interfaces (GUIs) in MATLAB[®], the ATD environment offers access to a variety of multi-body solutions, in addition to conic arcs. User interaction with plots allows for point-and-click arc selection, as well as interactive trajectory ‘clipping’, in which the desired arc along a longer trajectory may be isolated. A general overview of the ATD strategy is summarized as follows:

1. Select desired three-body system
2. Compute and select trajectory arcs of interest
3. Store any desirable arcs within ‘arc list’
4. Arrange all arcs within arc list into appropriate sequence for final design
5. Distribute nodes along each arc to facilitate differential corrections processes, and save data
6. Load saved data into differential corrections environments
7. Apply desired constraints, transition solution to ephemeris model, and save converged data as GMAT script file
8. Load saved data into GMAT and reconverge end-to-end result

In items 1-4, various trajectory options may be efficiently and rapidly explored within the interactive design environment. Once a design is selected, it is modified via steps 5-7 to include additional constraints and to transition the solution to a higher-fidelity ephemeris model. Finally, in step 8, the solution is reconverged within GMAT, where the end-to-end ephemeris solution can be subsequently employed for further analysis and to support other activities.

Trajectory Design Employing ATD: Sample Transfer to a Lunar Distant Retrograde Orbit

To demonstrate the design strategies employed within ATD, it is useful to begin with a relatively simple design goal. Consider a trajectory design concept to transport a spacecraft from a 200-km Low-Earth Orbit (LEO) to a Distant Retrograde Orbit (DRO)^{10, 14} in the vicinity of the Moon. The ATD design space, depicted in Figure 1, offers access to a large assortment of orbit types within one mission design environment, thus facilitating exploration of trajectory designs that include various types of orbits. For example, sample members from the family of DROs about the Moon are pre-computed by Capdevila¹⁵ and are available within the ATD environment. In the following example, the ATD strategies are demonstrated to design a transfer from LEO to a DRO about the Moon.

*The development effort is supported, in part, by the IRAD program at NASA Goddard Space Flight Center.

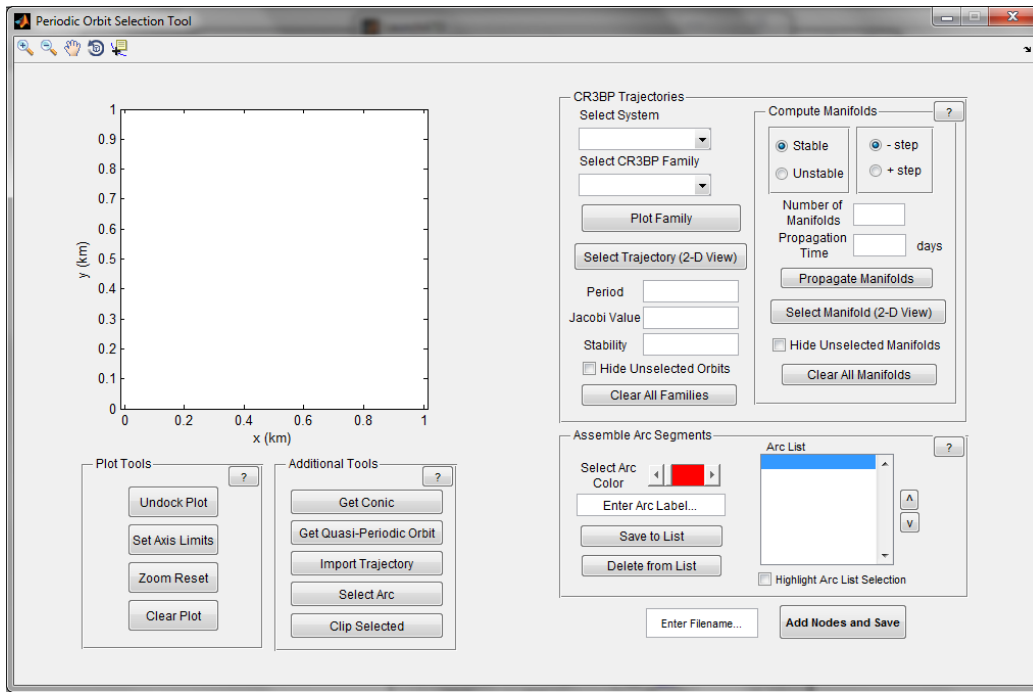
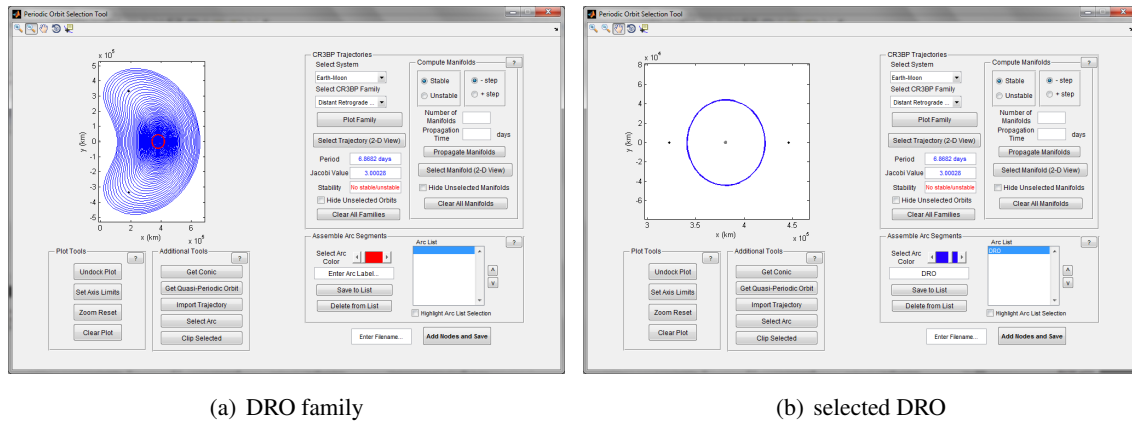


Figure 1. ATD design environment graphical user interface

Assembling a Trajectory Design To begin the design process, the desired three-body system is selected to be the Earth-Moon system. Trajectory arcs are then computed or selected, and the desired arcs are stored within an ‘arc list’ to be incorporated into the final design. For this example, the family of DROs is selected from a list of available orbit types, and a representative set of orbits from the family appears in blue in Figure 2(a). Recall that the view appears in the Earth-Moon



(a) DRO family

(b) selected DRO

Figure 2. Selecting a distant retrograde orbit from within the DRO family in the Earth-Moon system

rotating frame as the result of a previous selection. A particular member from the family is selected via point-and-click interaction with the plot, and appears in red. Saving this selected orbit to the arc list and removing the unselected family members from the plot, the selected DRO appears in

blue in Figure 2(b). The Moon appears near the center of the DRO, and the Earth-Moon L_1 and L_2 points appear as black dots to the left and right of the orbit. Stability information for any periodic orbit that is selected within ATD is available. The selected DRO is stable, and, therefore, does not possess stable or unstable invariant manifolds.

Without the availability of natural flow into/away from the orbit via the manifolds, an alternative transfer arc from the Earth is sought. For this example, a conic arc is employed to deliver the spacecraft to the selected DRO. Conic arcs centered on either primary are available to be computed within the ATD environment, and may be adjusted by the user. Selecting the ‘Get Conic’ button within the ‘Additional Tools’ panel, the GUI in Figure 3(a) appears (note that the selected DRO still appears on the plot in blue). The user may specify various characteristics for the conic arc

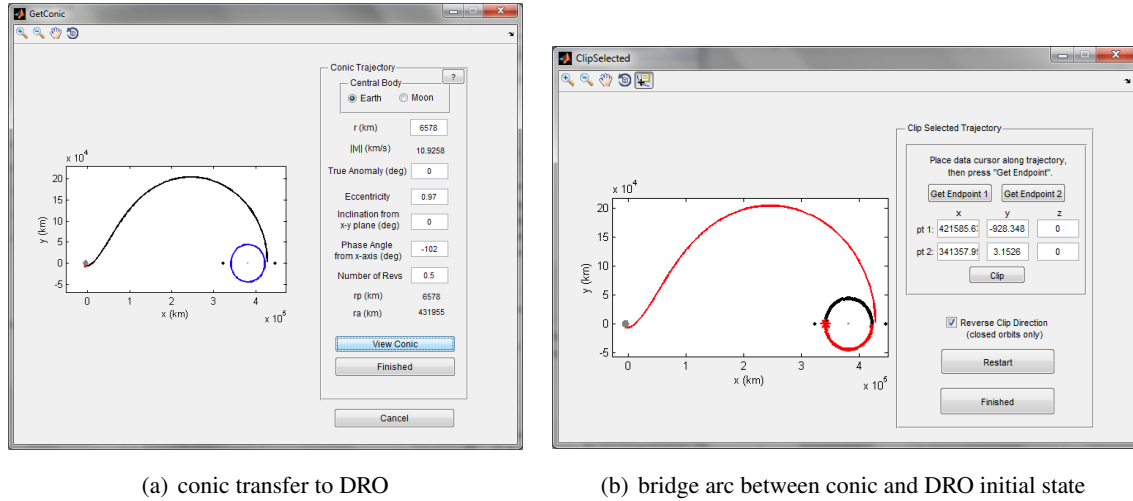


Figure 3. Incorporating a conic arc to transfer to a DRO, in addition to a bridge segment to adjoin the conic arc and DRO initial state

to achieve the desired transfer. Choosing the Earth as the central body, a transfer from a 200 km altitude LEO to the DRO is sought. Thus, a radius of $r = 6578$ km and a true anomaly of $\theta = 0^\circ$ are selected. The eccentricity value is modified until the transfer apogee is at roughly the same radius as a selected point on the DRO. Here, the selected point along the DRO is the x -axis crossing on the far side of the Moon (generally the most efficient entry point into this type of DRO) and the selected value for the eccentricity is $e = 0.97$. Because the DRO lies within the $x - y$ plane, the conic arc is also selected to possess 0° inclination relative to this plane. The phase angle measures the angle between the initial point along the conic, i.e., 6578 km perigee, and the x -axis in the Earth-Moon rotating frame. Changing this parameter to a value of -102° , the transfer apogee aligns closely with the selected x -axis crossing of the DRO. Finally, a value of 0.5 is selected for the number of revolutions, and the corresponding conic arc appears in black in Figure 3(a). The listed parameters may be adjusted until the transfer satisfies the user requirements, and the final conic arc is returned to the main design window of the GUI. The conic arc is saved to the arc list, where it is stored with the selected DRO. Once the desired arcs are stored within the list, they may be sorted into the appropriate order. In general, the final state along one arc may not align well with the initial state along another, thus, a ‘bridge’ segment may be required to reduce any discontinuity between two adjacent arcs. For example, while the conic arc aligns well with the x -axis crossing along the DRO on the far side of the Moon, the initial state along the precomputed DRO is actually the x -axis

crossing on the near side of the Moon. To bridge this gap, an arc from the DRO that links these two x -axis crossings may be selected and incorporated into the design. To do this, the DRO from the arc list is interactively selected and the ‘Clip Selected’ button is employed. A ‘clipping’ GUI appears, as demonstrated in Figure 3(b). The conic arc appears in red, and the selected orbit, i.e., the DRO, is plotted in black with the initial state appearing as a red star. Within this GUI, the desired start and end locations along the DRO are interactively selected to be the two x -axis crossings. By pressing ‘Clip,’ the red highlighted portion of the DRO appears that offers a link from the conic arc to the initial state along the DRO. Once the desired portion has been clipped, it is returned to the main GUI and added to the arc list. The final design appears in Figure 4 and includes: (1) the red conic arc producing transport from LEO to the vicinity of the DRO, (2) the green bridge that provides the link between the final state along the conic and the initial state along the DRO, (3)-(6) four copies of the DRO to include four revolutions along this final orbit. Note that the conic arc is plotted within

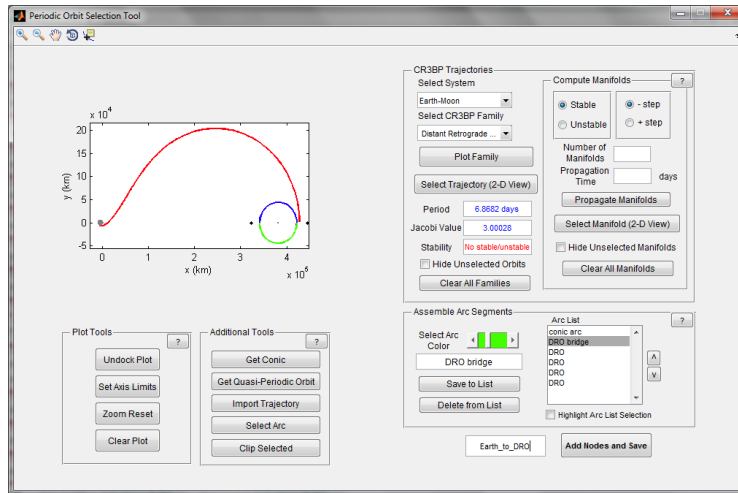
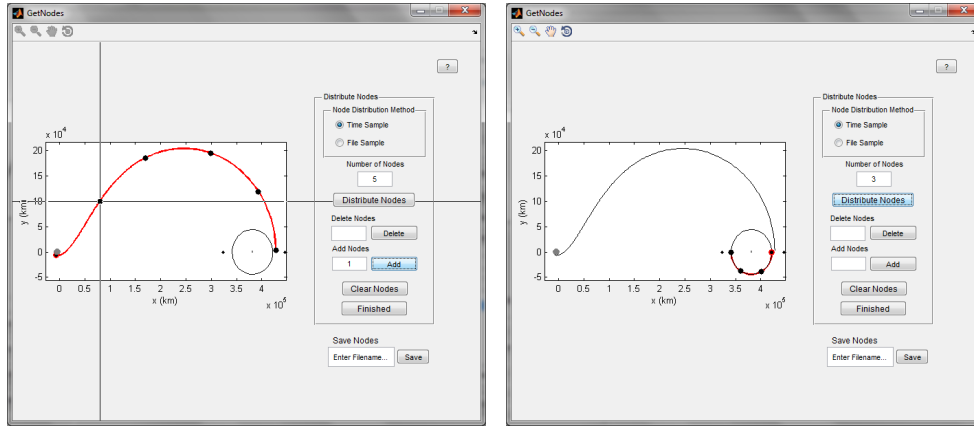


Figure 4. All desired arcs are stored in the arc list and are sorted into the appropriate order for the final design

the Earth-Moon rotating frame but the data are from the two-body problem. To this point, items 1-4 from the ATD strategy are completed. The final four items allow the solution to be transitioned into a higher-fidelity model, and, ultimately, to be reproduced in GMAT.

Transitioning the Final Design to an Ephemeris Model Once the final trajectory design is complete, a differential corrections process that ensures continuity along the path, in addition to any other desired constraints, is vital. Within the ATD differential corrections environments, constraints are interactively applied to the trajectory and the solution is reconverged in a unified dynamical model. To facilitate convergence in the corrections process, it is useful to distribute nodes or patch points along each arc to reduce integration times and, therefore, sensitivities. Upon saving the data associated with the trajectory design in Figure 4, the user is prompted to add nodes to each arc. The process of adding nodes is interactive; the user selects the number of nodes in addition to the method of distribution for the nodes (methods currently include equal distribution in time, and equal distribution within the data output from the numerical integration of each arc to accommodate regions of higher sensitivity), and is also able to add and delete nodes via point-and-click interaction. As an example, four nodes are equally distributed in time along the conic arc in Figure 5(a), and one additional node is interactively added between the first and second nodes. Nodes in the figure are

represented as black dots. The final state along the trajectory is additionally plotted as a black dot, although this point will not be included as a node in the data output. Three nodes are selected to be equally distributed in time along the conic to DRO bridge arc, as demonstrated in Figure 5(b). Finally, six nodes are distributed equally in time along each revolution of the DRO. The final state along the *final* trajectory arc in the design is always included as an additional node so that constraints may be applied at this terminal point. The data is saved in a *.mat file, and is then available to either reload into the design GUI for further modifications, or to be loaded into a differential corrections environment. Two ATD differential corrections environments appear in Figure 6. The

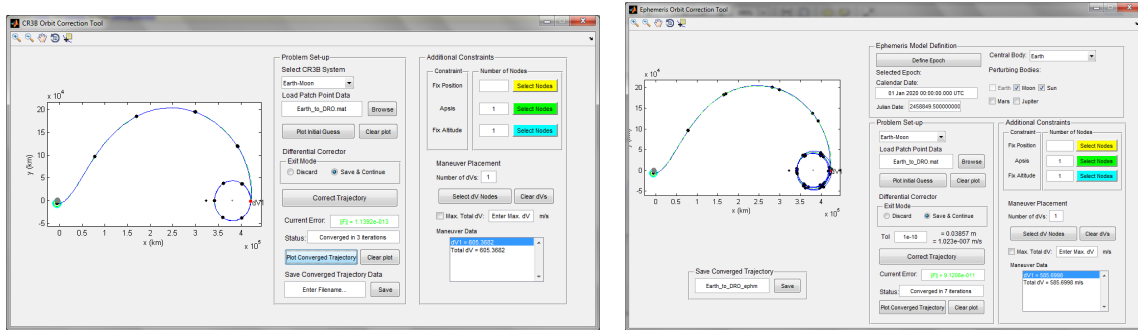


(a) adding nodes to conic arc

(b) adding nodes to conic bridge

Figure 5. Nodes are distributed along each arc within the final assembled trajectory design to aid in differential corrections processes

GUI in Figure 6(a) allows the user to apply constraints within the CR3B model, while the environment in Figure 6(b) facilitates the transition of the solution to a higher-fidelity ephemeris model. Within each differential corrections environment, constraints are interactively selected and applied, and any desired maneuvers are added and positioned via point-and-click selection. The available constraints in the GUIs in Figure 6 include fixing the location of a node, enforcing the condition that a particular node be an apsis, and constraining the altitude at a given node, although any additional



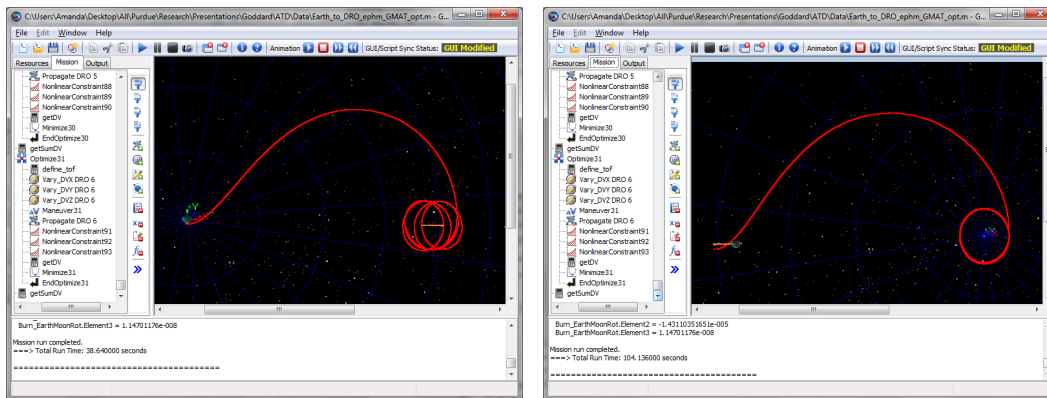
(a) corrected in CR3B model

(b) corrected in Sun-Earth-Moon ephemeris model

Figure 6. Applying differential corrections to compute a continuous transfer between the Earth and a DRO

desired constraints could be incorporated into the GUI environment. These constraints may be ap-

plied to multiple nodes along the trajectory. Velocity continuity is enforced between any arcs where maneuvers are not allowed, and position continuity is enforced between all arcs. For this example, the initial state is constrained to correspond to a 200-km altitude perigee. The corrected paths are computed within the CR3B model and a Sun-Earth-Moon ephemeris model, and are plotted in blue in Figures 6(a) and 6(b). A single maneuver is permitted to link the conic arc to the DRO, and the magnitude of this maneuver is 605.4 m/s for the CR3B model and 585.7 m/s in the ephemeris model. It is possible to reduce the magnitude of this maneuver using a constraint on the maximum value of the total Δv , however, no constraint on the maneuver size is included in this example. Finally, the ephemeris solution is saved within the ATD corrections environment and a script file is internally produced that is accessed via GMAT. This script file provides the transition from the ATD environment in MATLAB, to the GMAT mission design environment. Opening the output in GMAT, each node position along the ephemeris path is targeted using optimization to reduce the Δv required at each node. Running this script file reconverges the solution within GMAT, and the resulting solution appears in Figure 7. The reconverged solution requires 586.16 m/s and corresponds to a 36.6 day total time-of-flight. While the example in Figure 7 offers a relatively simple



(a) Earth-centered rotating view

(b) Moon-centered rotating view

Figure 7. Final converged transfer from Earth to a sample DRO is transitioned to GMAT

transfer, other transfer designs exist.^{14, 16, 17} The interactive design process available within the ATD environment allows the user to rapidly explore alternative design options and to gain insight into the solution space. In the following examples, more complicated designs are assembled to demonstrate the design capabilities that are available when utilizing ATD strategies.

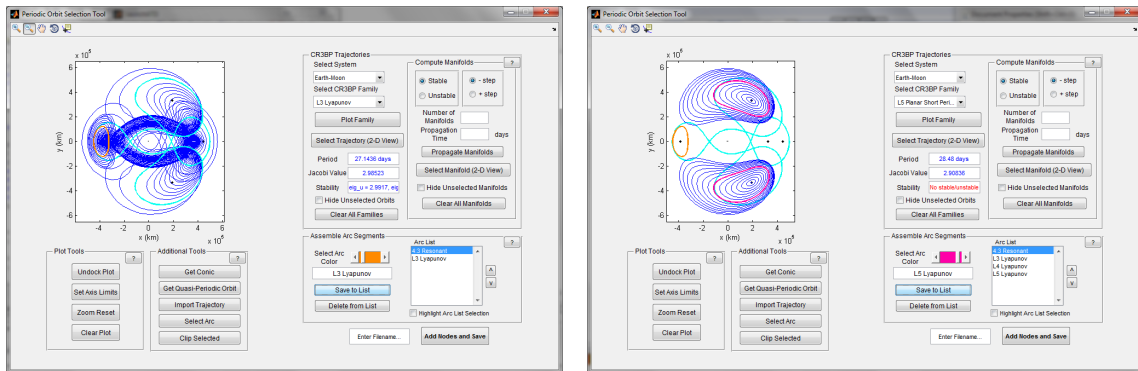
APPLICATION OF ADAPTIVE TRAJECTORY DESIGN STRATEGIES TO THE DESIGN OF TOURS IN THE EARTH-MOON SYSTEM

Using the strategies presented in the previous section, it is a simple and efficient process to explore the design space and to compute trajectory designs for a variety of scenarios. In the following examples, the ATD environment is explored for application to tours within the Earth-Moon system. The roles of various orbits in facilitating transport in the Earth-Moon system are demonstrated, emphasizing the value in design tools that offer access to a composite view of a variety of orbit types.

Tour of Libration Point Orbits Using Resonant Orbits

In addition to considering invariant manifolds associated with libration point orbits, a variety of different orbit types are useful when designing transfers in the Earth-Moon system. For example, the role of resonant orbits in the design of libration point tours in the Earth-Moon system has been previously demonstrated by Vaquero and Howell.^{18,19} Incorporating families of resonant orbits into the ATD environment, the process to reproduce similar tours is straightforward. Many resonant orbits, such as members of the 4:3 resonant family, visit the regions of Earth-Moon space in the vicinity of the L_3 - L_5 libration points, and are, therefore, useful in the design of tours. In the following example, a tour of the L_3 , L_4 , and L_5 points is constructed using a selected member of the Earth-Moon family of 4:3 resonant orbits to facilitate the transfers.

To begin, consider the families of 4:3 resonant orbits and L_3 Lyapunov orbits, plotted in blue in Figure 8(a). Because the motion of these orbits is similar in the vicinity of L_3 , it is difficult to identify the L_3 family from this view. Zooming in on the region near L_3 , it is easier to distinguish the families and to select orbits of interest. Sample Lyapunov and resonant orbits are selected from within the families, and are plotted in orange and cyan, respectively. While a different pair of orbits could be selected, these sample orbits are identified because it is visually apparent that the orbits are roughly tangent to one another as they cross the x -axis, indicating that a reasonable transfer is possible. Next, assuming the selected 4:3 resonant orbit is employed to design the tour, the L_4 and L_5 Lyapunov orbits are selected. In Figure 8(b), sample members from the families of planar

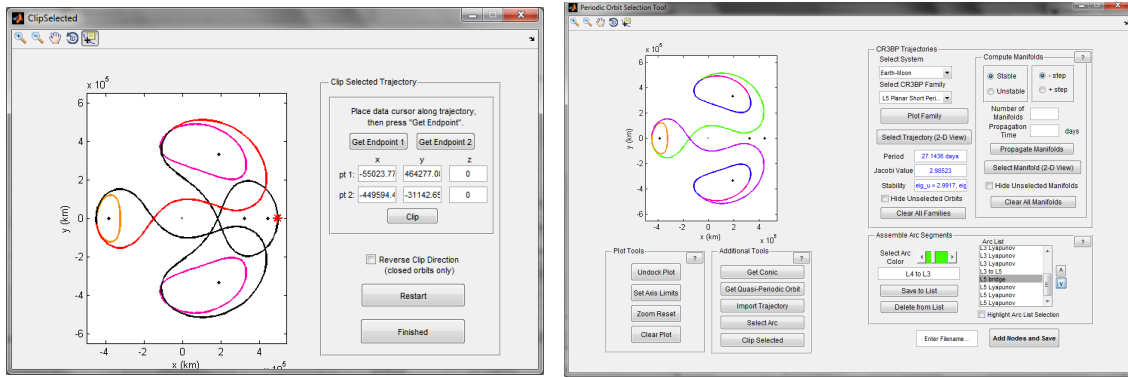


(a) selected 4:3 resonant and L_3 orbits

(b) selected L_4 and L_5 orbits

Figure 8. Building a tour of the L_3 , L_4 , and L_5 points using resonant orbits in the Earth-Moon system

L_4 and L_5 Lyapunov orbits are plotted in blue. The cyan 4:3 orbit appears tangent to the pair of selected pink orbits in the vicinity of L_4 and L_5 , thus, these pink orbits are incorporated into the tour. Each of the selected orbits (L_3 - L_5 Lyapunovs and 4:3 resonant) is stored in the arc list in the lower right of Figure 8(b). In their current form, these orbits comprise a discontinuous set of trajectory arcs. It is necessary, then, to link these arcs so that the resulting trajectory produces a continuous tour of the desired libration points. For example, the portion of the 4:3 resonant orbit that supplies a connecting arc between the L_4 and L_3 libration point orbits is isolated using the clipping technique. The desired start and stop locations are interactively selected along the orbit, and all excess is removed. This process is demonstrated in Figure 9(a), where the entire resonant orbit appears in black and the red segment along the resonant orbit is clipped to supply the transfer from L_4 to L_3 . Repeating the clipping procedure to generate the transfer arc between L_3 and L_5 , a



(a) clipped resonant orbit arc

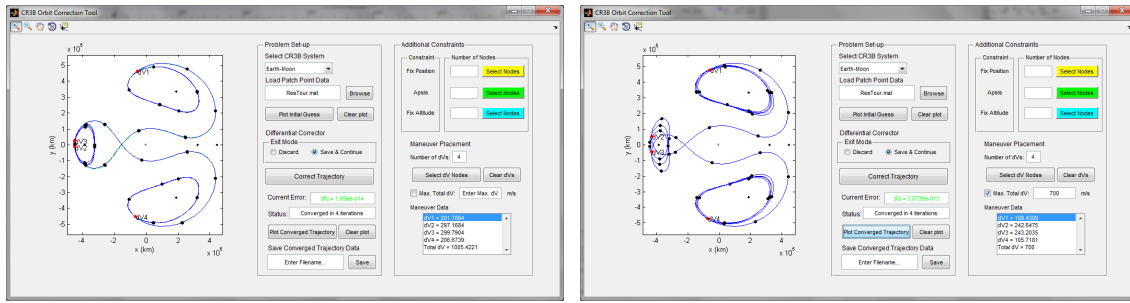
(b) final tour design

Figure 9. A tour of the L_3 , L_4 , and L_5 points is constructed using resonant orbits in the Earth-Moon system

baseline for the final tour appears in Figure 9(b). Note that bridge arcs, plotted in blue, are isolated using the clipping procedure and are included to reduce discontinuities between the resonant orbit transfer arcs and the initial states along the precomputed L_4 and L_5 orbits. Four copies of each libration point orbit are included in this baseline so that multiple revolutions along each orbit are incorporated. The final itinerary proceeds as follows: (1)-(4) L_4 Lyapunov orbit in pink, (5) L_4 bridge arc in blue, (6) resonant transfer arc in green, (7)-(10) L_3 Lyapunov orbit in orange, (11) resonant transfer arc in purple, (12) L_5 bridge arc in blue, and (13)-(16) L_5 Lyapunov orbit. Once all arcs are assembled and properly sorted, nodes are distributed along each arc and the data is saved to a *.mat file to be loaded into the interactive differential corrections environments.

With the discontinuous baseline assembled and sampled, the data for the particular mission scenario is loaded into the CR3B corrections environment depicted in Figure 10. Four locations are interactively selected along the path, corresponding to user-specified locations where maneuvers will be allowed. Position continuity is enforced along the trajectory, and the corrected solution appears in blue in Figure 10(a). The corrected trajectory includes maneuvers totalling 1005.4 m/s. Using this converged solution as the new baseline, and applying an upper limit on the total allowed Δv , an interactive continuation strategy is facilitated to reduce the required Δv for the end-to-end trajectory. Using this procedure, the total Δv is reduced to 700 m/s, and the resulting tour, as constructed in the CR3B model, appears in Figure 10(b). The total required Δv can be further reduced, however, the L_3 orbit shape begins to experience significant changes. With the desired constraints applied to the baseline trajectory, this solution is transitioned to an ephemeris model. Reconverging the solution from Figure 10(b) in a Sun-Earth-Moon model, assuming an epoch of January 1, 2020 00:00:00.000 UTC, the resulting tour appears in Figure 11(a). The ephemeris path requires a total Δv of 680.1 m/s. Saving the ephemeris data from this GUI, the script file output is loaded into GMAT, and the reconverged tour requires 680.6 m/s, comprised primarily of four impulsive maneuvers of magnitude equal to 33.8 m/s, 293.9 m/s, 227.2 m/s, and 125.3 m/s. The time-of-flight along the tour totals 345.7 days. Of course, other epochs and constraints can easily be accommodated.

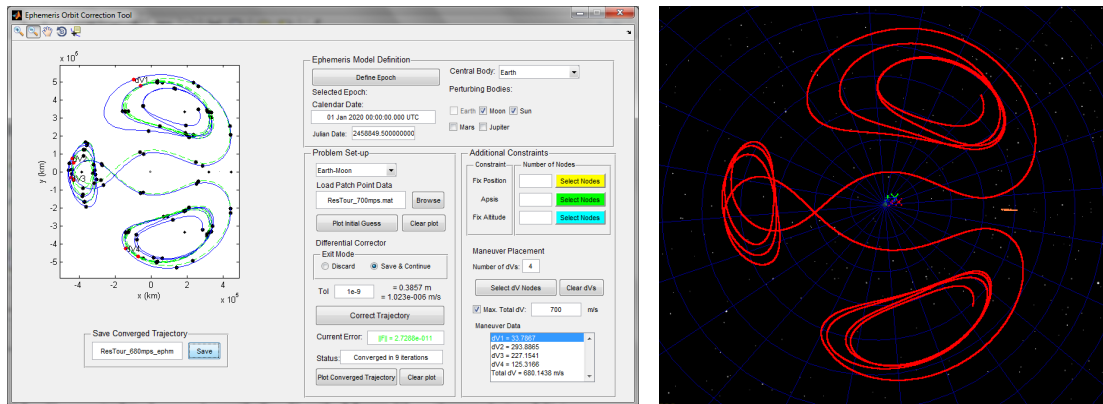
Exploiting resonant orbits, a tour of the L_3 - L_5 Earth-Moon libration points is straightforward to design within the ATD environment. With the resonant, L_3 , L_4 , and L_5 orbit families all available within one design setting, the process of selecting desirable orbits to generate the tour is intuitive. An interactive interface for arc selection and manipulation allows the user to quickly isolate trajec-



(a) correcting discontinuous path

(b) reducing total Δv

Figure 10. Differential corrections schemes and continuation methods allow for enforcement of constraints and reduction of total required Δv



(a) corrected Sun-Earth-Moon ephemeris path

(b) ephemeris path in GMAT

Figure 11. Corrected ephemeris path for an Earth-Moon libration point orbit tour

tory arcs of interest, and to assemble the individual arcs into an end-to-end mission design.

Accessing Libration Points via Vertical Orbit Manifolds

The families of vertical orbits and their associated invariant manifolds cover an expansive region of the space in the Earth-Moon system. For example, Haapala and Howell²⁰ compute a variety of homoclinic connections (free transfers) associated with vertical orbits in the vicinity of L_1 and L_2 ; two sample connections appear in Figures 12(a)-12(b). Similar connections are reproduced within the ATD environment by employing the stable and unstable manifolds asymptotic to vertical orbits with energy levels near the values employed by Haapala and Howell. The selected vertical orbit nearby the energy level associated with homoclinic connection 2 appears in Figure 13(a). Manifolds are straightforward to compute within ATD for any periodic orbit by selecting a desired number of trajectories to represent the manifold surface, as well as the integration time. For example, 50 sample arcs along the unstable manifold surface that flows away from the vertical orbit and toward the Earth are propagated for 75 days, and are plotted in magenta in Figure 13(b). A sample stable manifold appears in green. A particular unstable manifold arc, plotted in red, is selected from the collection and is clipped so that the final position is near the final state along the stable manifold. Together, the green and red arcs form the initial guess for the transfer leg of a homoclinic connection

associated with the L_2 vertical orbit. Using ATD to assemble the initial guesses and reconverging the connections in GMAT, the resulting transfers appear in Figures 12(c)-12(d) and require 0.22 m/s and 213.9 days, and 0.33 m/s and 171.3 days, respectively. Both transfers depart from an

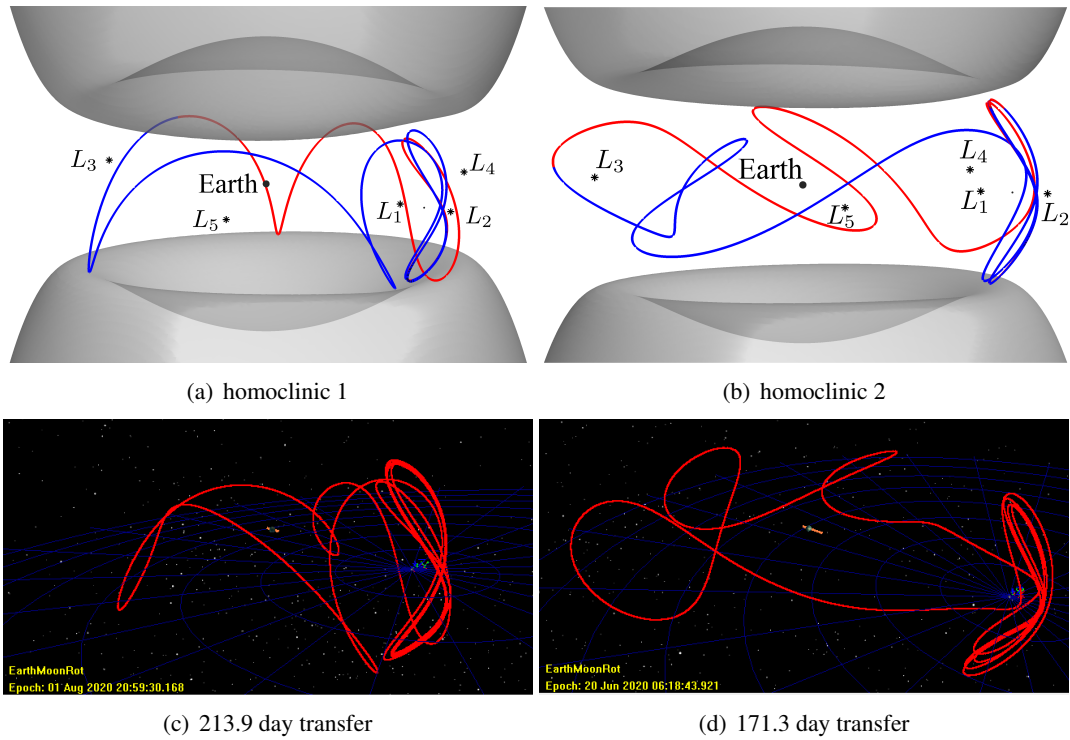


Figure 12. A pair of homoclinic connections associated with L_2 vertical orbits are reproduced using ATD

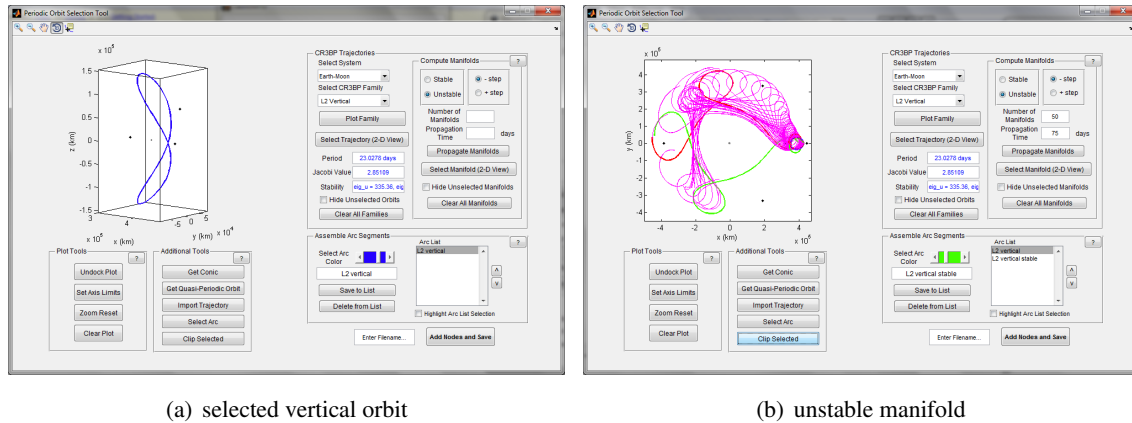


Figure 13. Reproducing a homoclinic connection within ATD

L_2 vertical orbit and traverse the Earth-Moon system before returning back to the vertical orbit. Because the transfer in Figure 12(d) includes a single revolution about L_3 , it offers the potential to transfer between the L_2 vertical orbit and an L_3 libration point orbit. In this example, tours that incorporate both the L_2 vertical orbit and an L_3 orbit are constructed within the ATD environment.

To design a three-dimensional transfer between L_2 and L_3 libration point orbits, an L_3 orbit that is nearly tangent to the homoclinic transfer in Figure 12(d) is sought in an effort to reduce the total required Δv . While the L_3 families of halo and vertical orbits do not include any orbits that align well with the connection in Figure 12(d), an L_3 orbit is simple to construct using clipping to isolate the L_3 revolution from the homoclinic transfer, as demonstrated in Figure 14(a). Here, the selected unstable and stable manifolds employed to compute the homoclinic connection appear in pink and green. A section from the unstable/stable manifold is clipped out and appears in cyan/blue. These clipped portions supply an approximation for a single revolution about L_3 . To include multiple revolutions, four copies of the single revolution are concatenated, and the discontinuous baseline is corrected using the CR3B corrections tools to form a continuous, maneuver-free orbit in the vicinity of L_3 . The corrected orbit, plotted in Figure 14(b), is then reloaded into the ATD environment for use in the design of a transfer between L_2 and L_3 . After importing the L_3 orbit from Figure

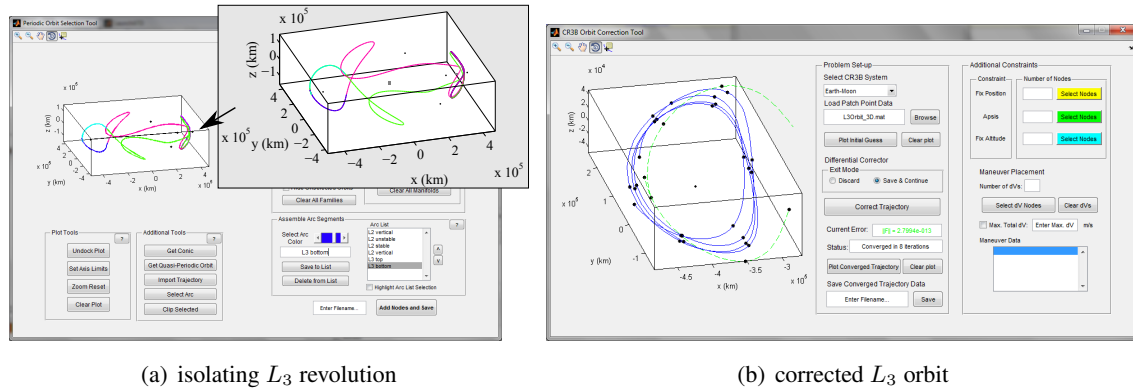


Figure 14. An L_3 orbit is constructed by sampling a portion of an L_2 vertical homoclinic connection

14(b) back into the design GUI, the portion of the vertical homoclinic path that allows transport between L_3 and the L_2 vertical, i.e., the green stable manifold, is selected and appears in green in Figure 15(a), with the L_3 orbit in blue. Three revolutions along the vertical orbit are additionally included, and appear in purple. This baseline trajectory is corrected for continuity in the CR3B model, allowing a single maneuver to link the L_3 orbit to the vertical orbit stable manifold. The magnitude of the maneuver is reduced from 241.7 m/s to 100 m/s by applying an upper limit on the total allowed Δv within the differential corrections process. Finally, the solution is transitioned to an ephemeris model and is reconverged within GMAT. The resulting 210.6 day trajectory requires a single maneuver of 100.5 m/s and is plotted in Figure 15(b). The design appearing in Figure 15 is straightforward to modify within the ATD environment. Sample trajectory designs with modified itineraries appear in Figure 16. The design in Figure 16(a) incorporates a transfer from the L_2 vertical to the L_3 orbit, via the vertical orbit unstable manifold, before a return back to the L_2 vertical orbit, and requires a total of 200.3 m/s to enter and depart the L_3 orbit. A departure leg from a 200-km LEO is included in the path displayed in Figure 16(b), and two maneuvers of 657.4 m/s and 86.2 m/s are permitted to transfer in and out of the L_3 orbit.

A variety of solution types prove useful in the design of tours in the Earth-Moon system. Using the ATD environment, a homoclinic connection associated with an L_2 vertical orbit is reproduced. Arcs from the homoclinic solution are manipulated within the design interface to produce a connection between L_2 and L_3 , and the process to modify the itinerary is straightforward and efficient.

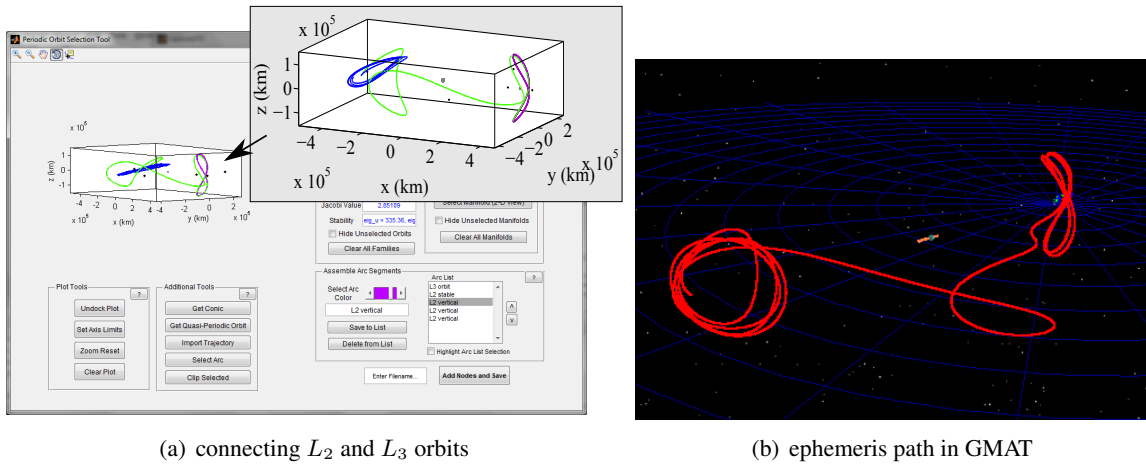


Figure 15. A transfer from an L_3 orbit to the L_2 vertical is designed in the Earth-Moon system and corrected in a Sun-Earth-Moon ephemeris model

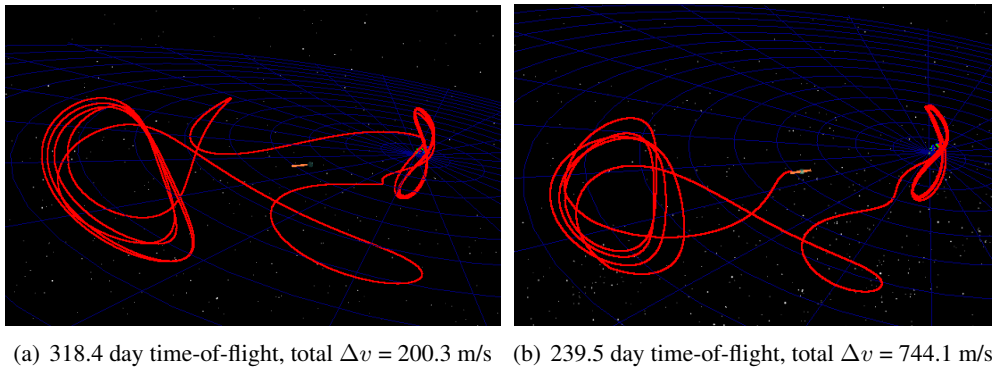


Figure 16. A transfer between the L_3 and L_2 orbits in the Earth-Moon system is modified within ATD to include additional arcs

RELATING ORBIT STRUCTURES NEAR THE MOON IN THE EARTH-MOON SYSTEM

A design environment that offers a composite view of multi-body orbits is useful, not only to explore a variety of mission design options, but also to gain insight into the relationships between different orbit types. The application of stable and unstable manifolds associated with orbits in the vicinity of L_1 and L_2 to locate transfers in the vicinity of the smaller primary has been demonstrated by previous researchers (e.g., Conley,²¹ Koon et al.,⁹ Gómez et al.,²² and Parker et al.¹¹). Parker et al. additionally demonstrate the relationship between Distant Prograde Orbits (DPOs) and libration point orbits, and compute heteroclinic chains and complex periodic orbits that include each orbit type. Transfer trajectories for the P1 and P2 spacecraft from the ARTEMIS¹² mission incorporate stable and unstable manifolds associated with libration point orbits in the vicinity of L_1 and L_2 . A merged view of the P1 and P2 mission orbits with members from the family of DPOs in the Earth-Moon system reveals an association between these orbit structures, and it is apparent that the transfers employed by the ARTEMIS spacecraft inherit characteristics associated with nearby DPOs. Exploiting the manifold structures associated with DPOs, a transfer that closely resembles those executed by the ARTEMIS P1 spacecraft is computed.

Interaction between ARTEMIS P1 Orbit and Distant Prograde Orbits

ARTEMIS was the first libration point mission in the Earth-Moon system. Near the end of the THEMIS mission, the THEMIS spacecraft P1 and P2 were flown to the vicinity of the Moon where they were maintained in large quasi-halo orbits about the Earth-Moon L_1 and L_2 points before entering long-term lunar orbits.²⁶ The transfer between orbits in the vicinity of L_2 and L_1 for the P1 spacecraft is imported into the ATD environment and appears in blue in Figure 17. Both planar

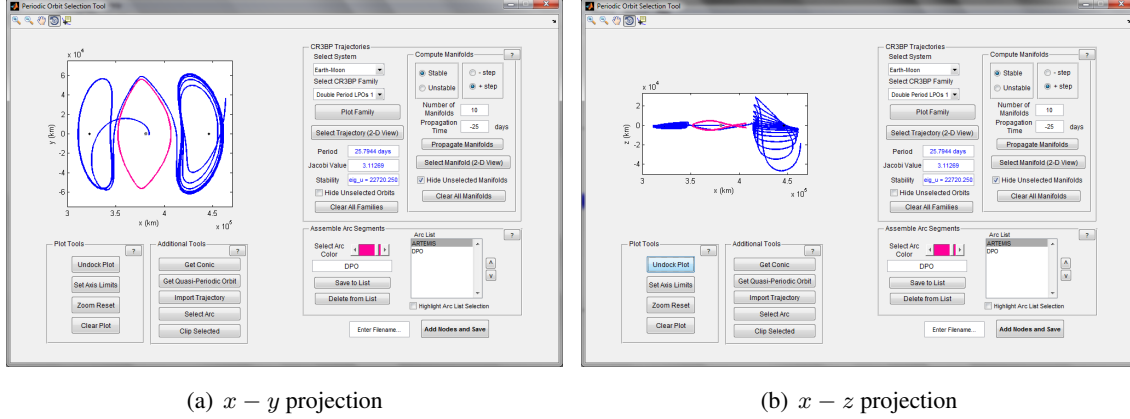


Figure 17. ARTEMIS P1 transfer between L_2 and L_1 libration point orbits

and three-dimensional DPOs exist.^{10,20,23,24} Comparing the transfer arc between the libration point orbits to a sample three-dimensional DPO, plotted in pink, qualitative similarities are apparent. By including various orbit types within one mission design setting, the relationship between transfers between L_1 and L_2 libration point orbits and the family of DPOs may be explored.

Members from the family of DPOs near the energy level associated with the ARTEMIS trajectories are unstable and, therefore, possess stable and unstable manifolds that asymptotically approach and depart the orbit. Exploiting the manifold structures associated with planar DPOs, heteroclinic chains (free transfers) are computed that are qualitatively similar to the transfers executed by the ARTEMIS spacecraft. A plot displaying the ranges for the Jacobi constant values associated with the planar family of DPOs, as well as the L_1 Lyapunov and L_2 Lyapunov orbits, appears in Figure 18. For a periodic orbit, the associated monodromy matrix possesses eigenvalues $\lambda_1 = \lambda_2 = 1$, $\lambda_3 = 1/\lambda_4$ ($|\lambda_3| \geq 1$), $\lambda_5 = 1/\lambda_6$ ($|\lambda_5| \geq 1$), and the stability index may be computed as $\nu = \frac{1}{2}(\lambda_i + 1/\lambda_i)$.^{19,25} Note that λ_i may be complex. For a *planar* periodic orbit, the monodromy matrix possesses eigenvectors \bar{v}_3, \bar{v}_4 with a zero component in z and \dot{z} . Then, the stability parameter ν_{2D} is defined $\nu_{2D} = \frac{1}{2}(\lambda_3 + 1/\lambda_4)$. For eigenvectors \bar{v}_5, \bar{v}_6 that possess zero x, y, \dot{x}, \dot{y} components, $\nu_{3D} = \frac{1}{2}(\lambda_5 + 1/\lambda_6)$. Values of ν may range from $(-\infty, -1]$ and $[1, \infty)$. The parameters ν_{2D} and ν_{3D} are represented in Figure 18 for sample members from the family of DPOs: the value of ν_{3D} is mapped to the colorbar and the values x_0 and C are represented by a colored marker for each sample orbit (here, x_0 indicates the value of x along the orbit at the x -axis crossing for which $\dot{y} < 0$); a gray vector of magnitude $|\nu_{2D}|$ is attached to each colored marker. An orbit for which $|\nu_{2D}| > 1$ is unstable and possesses planar stable and unstable invariant manifolds that provide asymptotic flow into and away from the orbit. The black box indicates the region on the plot for which all three orbit types exist and possess a value of $|\nu_{2D}| > 1$. For any value of Jacobi constant within this region, free transfers exist between the families of L_1 and L_2 Lyapunov orbits as well as

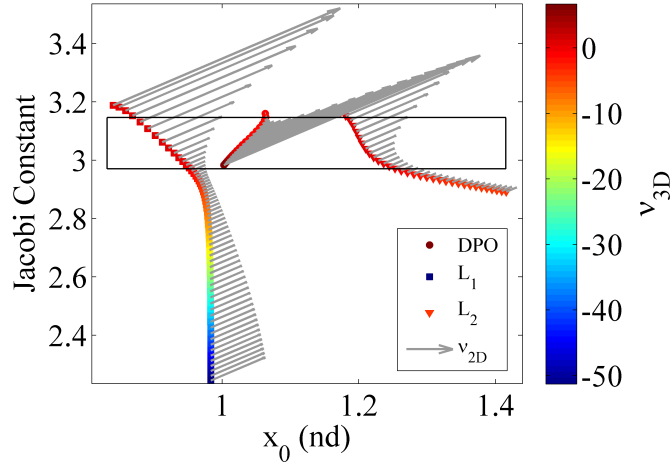
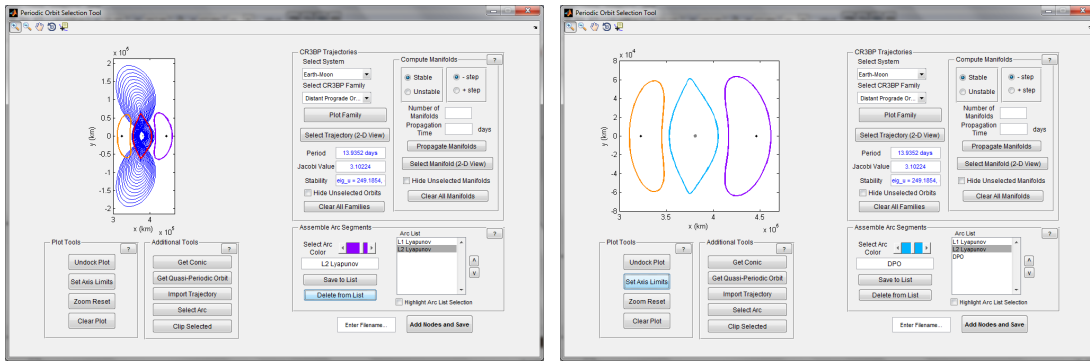


Figure 18. Transfers between L_1 and L_2 Lyapunov orbits and Moon-centered DPOs are available for a range of energy levels

the family of DPOs.

The trajectories employed for the ARTEMIS spacecraft correspond to Jacobi constant values within the range indicated by the black box in Figure 18, and serve as a useful example to demonstrate the relationship between the families of Lyapunov and distant prograde orbits. To examine this relationship, planar Lyapunov orbits of a similar y -amplitude to the libration point orbits from the ARTEMIS P1 path are first computed. Within the ATD design environment, an interactive targeting algorithm produces the option to locate a libration point orbit possessing a desired in-plane or out-of-plane amplitude. The maximum y -amplitudes associated with the P1 L_1 and L_2 libration point orbits are 58816 km and 63520 km, respectively.²⁶ Within the targeting tool, a Lyapunov/halo/vertical orbit can be computed for a user specified y - (Lyapunov or halo orbits) or z -amplitude (halo or vertical orbits). For this analysis, Lyapunov orbits corresponding to y -amplitudes of 59000 km and 63500 km are computed in the vicinity of L_1 and L_2 , respectively. These orbits correspond to Jacobi constant values of $C = 3.10007$ and 3.10172 , consistent with the highlighted Jacobi constant range in Figure 18. The selected Lyapunov orbits are saved to the arc list, and appear in Figure 19(a) in orange and purple. In addition, sample members from a precomputed family of DPOs are plotted in blue in the figure, with a particular orbit from the family selected and plotted in red. This orbit corresponds to a Jacobi constant value of $C = 3.10224$, and is plotted in light blue in Figure 19(b), in addition to the selected L_1 and L_2 Lyapunov orbits. The periods of the L_1 Lyapunov, L_2 Lyapunov, and distant prograde orbits are 13.6 days, 15.6 days, and 13.9 days.

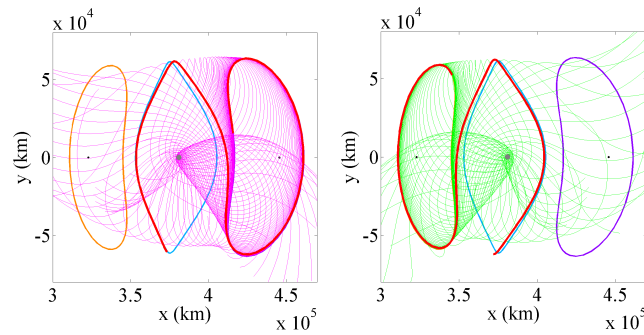
The three selected orbits have not been computed for precisely the same value of Jacobi constant, however, they correspond to relatively close values of C and prove useful to gain insight into the behavior of the ARTEMIS P1 transfer between L_2 and L_1 . Within the ATD design GUI, manifolds associated with each of the selected periodic orbits are computed. For example, 50 sample trajectories along the unstable manifold associated with the L_2 Lyapunov are propagated for 25 days; the figure is ‘undocked’ from the ATD GUI and appears in Figure 20(a). A particular trajectory is interactively selected, and appears in red. The selected manifold is qualitatively similar to the light blue DPO, that is, the manifold closely shadows the DPO over the integration time, indicating that a nearby heteroclinic connection between the Lyapunov and DPO may exist. Additionally, sample



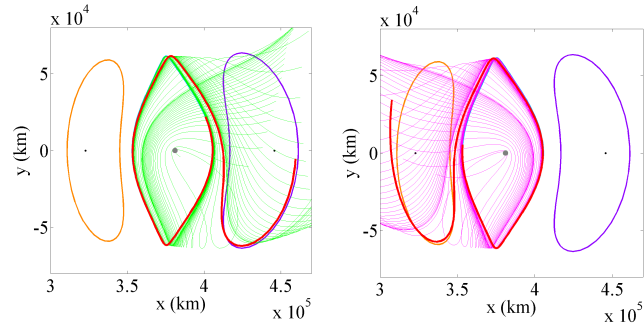
(a) selecting a DPO

(b) all three selected orbits

Figure 19. Selecting orbits with amplitudes similar to those employed for the ARTEMIS P1 trajectory



(a) L_2 Lyapunov unstable mani- (b) L_1 Lyapunov stable manifold
fold

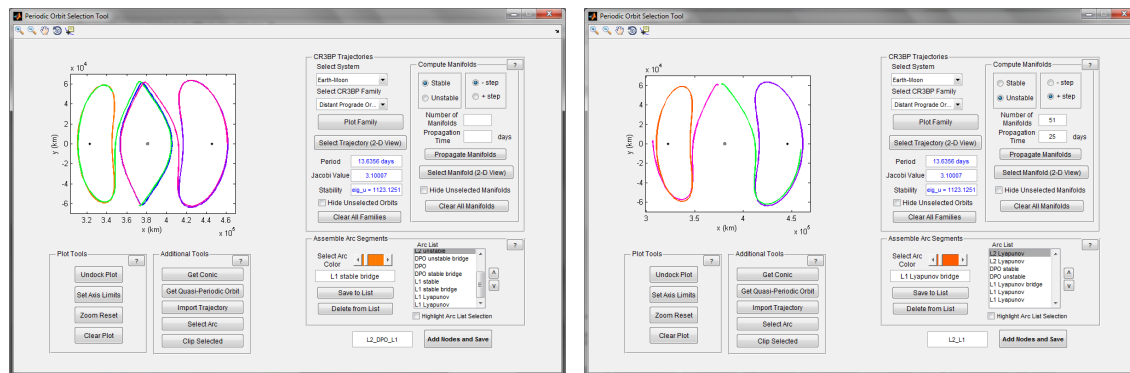


(c) DPO stable manifold (d) DPO unstable manifold

Figure 20. Manifolds associated with Lyapunov orbits and DPOs indicate the existence of a nearby heteroclinic chain

stable manifolds asymptotic to the L_1 Lyapunov orbit and DPO are computed and appear in Figures 20(b) and 20(c), respectively; sample trajectories along the unstable manifold associated with the DPO are plotted in Figure 20(d). A clear association between the manifolds associated with the Lyapunov orbits and the central DPO is observed. Specifically, the selected manifolds, plotted in red, asymptotic to the Lyapunov orbits additionally shadow the DPO, and the DPO manifolds that

are plotted in red inherit characteristics associated with the Lyapunov orbits. Thus, a heteroclinic chain is sought to produce a free transfer from the L_2 Lyapunov to the DPO, and from the DPO to the L_1 Lyapunov. A heteroclinic chain with the itinerary L_2 Lyapunov \rightarrow DPO \rightarrow L_1 Lyapunov is assembled from the manifolds plotted in Figures 20(a)-20(b), and the transfer design appears in Figure 21(a). The transfer, as converged within a Sun-Earth-Moon ephemeris model, appears in Fig-



(a) L_2 -DPO- L_1 design

(b) L_2 - L_1 design

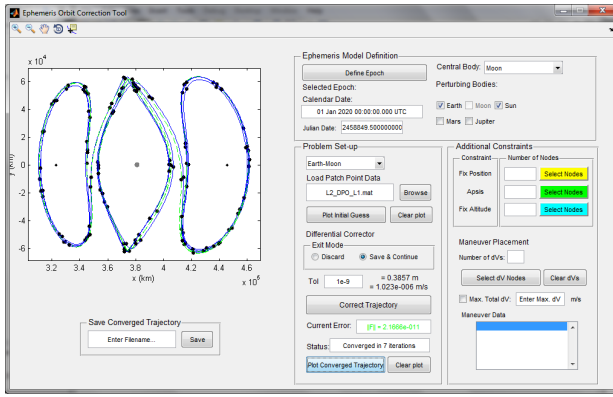
Figure 21. Assembled transfer designs between L_2 and L_1 Lyapunov orbits

ures 22(a)-22(b) and requires a total time-of-flight of 143.2 days, including roughly two revolutions along each of the Lyapunov orbits as well as the DPO. Within GMAT, solar radiation pressure (SRP) is included in the force model, and the resulting transfer requires a total of 0.17 m/s, comprised of maneuvers with magnitudes on the order of 1×10^{-5} to 1×10^{-3} m/s. Without the inclusion of SRP, the total Δv is 0.12 m/s. Employing the DPO manifolds plotted in red in Figures 20(c)-20(d), a direct transfer between the L_2 and L_1 Lyapunov orbits is constructed and appears in Figure 21(b). The converged transfer in the Sun-Earth-Moon ephemeris model appears in Figure 22(c)-22(d). Including SRP, the reconverged GMAT solution requires a total of 0.10 m/s and 86.4 days, including two revolutions along each Lyapunov orbit totalling roughly 58 days. For all solutions, a start epoch of January 1, 2020 00:00:00.000 UTC is arbitrarily selected, and continuity in position is enforced to ~ 0.01 m. Note that the pulsation in the rotating frame has been removed in the plots in Figures 22(a) and 22(c) (i.e., the Earth, Moon, and libration points are fixed in these figures), however, the trajectories in Figures 22(b) and 22(d) are plotted in the pulsating rotating frame.

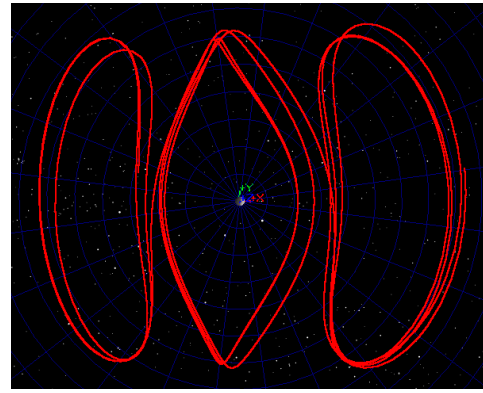
A design setting that offers a composite view of multi-body orbits is useful to gain insight into the relationships between various orbit types. Transfer trajectories for the P1 and P2 spacecraft from the ARTEMIS mission are qualitatively similar to nearby distant prograde orbits. Exploiting manifolds associated with members from the family of DPOs near the energy level associated with the ARTEMIS trajectories, transfers that closely resemble the ARTEMIS P1 transfer are efficient to design within the ATD environment.

CONCLUSIONS

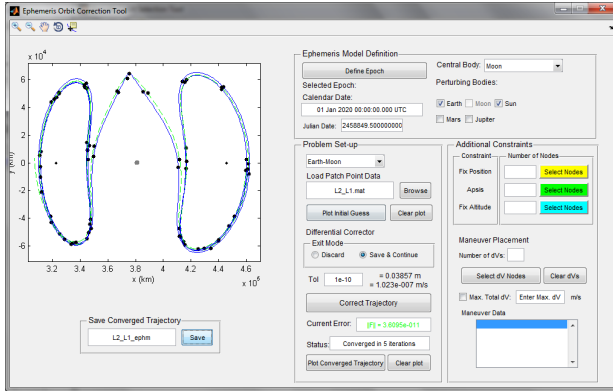
Improved flexibility in mission design tools is vital to enable the design of missions with increasingly complex requirements. Interactive and automated trajectory design tools provide an enhanced perspective of the design space and facilitate rapid exploration of a variety of design concepts. In this investigation, Adaptive Trajectory Design (ATD) strategies are demonstrated for mission design



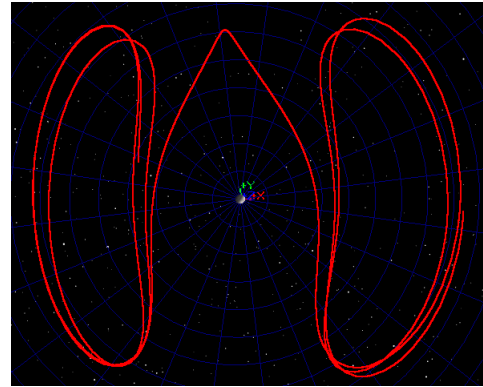
(a) L_2 -DPO- L_1 corrected ephemeris path



(b) L_2 -DPO- L_1 path in GMAT



(c) L_2 - L_1 corrected ephemeris path



(d) L_2 - L_1 path in GMAT

Figure 22. Corrected ephemeris path resembling the ARTEMIS P1 transfer

applications in the Earth-Moon system. Operating within a graphical user interface, the ATD tools facilitate the assembly of end-to-end mission designs via interactive selection of trajectory arcs with desirable characteristics. By enabling access to a large assortment of orbit types within one mission design environment, ATD offers the user a unique design perspective in which various mission design options may be explored, and the effectiveness of different orbits in meeting mission requirements may be evaluated. Sample mission designs are demonstrated, including a tour of the L_3 , L_4 , and L_5 libration points using resonant orbits as the transfer mechanism, and a transfer between orbits in the vicinity of L_2 and L_3 employing manifolds associated with an L_2 vertical orbit. Final designs are imported into NASA's General Mission Analysis Tool (GMAT), where the end-to-end ephemeris solution is reconverged and can be accessed in a mission setting for further analysis and to support other activities.

ACKNOWLEDGMENTS

Portions of this work have been accomplished at Purdue University as well as on-site at NASA Goddard. The authors appreciate the support of NASA Goddard Space Flight Center under Internal Research And Development (IRAD) grants NNX12AC57G and NNX13AE55G. Support through the Zonta International Amelia Earhart Fellowship is also appreciated. Many thanks to Lucia Capdevila, Ph.D. student at Purdue University, for her assistance with computations.

REFERENCES

- [1] K. C. Howell, and J. P. Anderson, "Generator's User's Guide, Version 3.0.2," IOM AAE-0140-012, July, 2001.
- [2] K. C. Howell, and J. J. Guzmán, "Generator," IOM AAE-0140-010, 2001.
- [3] M. Lo, "LTool Version 1.0G Delivery," JPL, IOM 00-2147, September, 2000.
- [4] J. M. Mondelo, E. Barrabés, G. Gómez, and M. Ollé, "Numerical Parametrizations of Libration Point Trajectories and their Invariant Manifolds," 23rd AAS/AIAA Space Flight Mechanics Meeting, Kauai, Hawaii, February, 2013. Paper No. AAS 07-321.
- [5] E. J. Doedel, and B. E. Oldeman, "AUTO-07P: Continuation and Bifurcation Software for Ordinary Differential Equations," January, 2012.
- [6] W. Schlei, "An Application of Visual Analytics to Spacecraft Trajectory Design," M.S. Thesis, School of Aeronautics and Astronautics, Purdue University, West Lafayette, Indiana, 2011.
- [7] D. J. Conway, and S. P. Hughes, "The General Mission Analysis Tool (GMAT): Current Features and Adding Custom Functionality," 4th International Conference on Astrodynamical Tools and Techniques, Madrid, Spain, May, 2010.
- [8] General Mission Analysis Tool Wiki, [Accessed August 1, 2013]. GMATcentral.org.
- [9] W. S. Koon, M. W. Lo, J. E. Marsden, and S. D. Ross, "Heteroclinic Connections Between Periodic Orbits and Resonance Transitions in Celestial Mechanics," *Chaos*, Vol. 10, 2000, pp. 427-469.
- [10] M. Hénon, "Numerical Exploration of the Restricted Problem. V. Hill's Case: Periodic Orbits and Their Stability," *Astronomy and Astrophysics*, Vol. 1, 2969. pp. 223-238.
- [11] J. S. Parker, K. E. Davis, and G. H. Born, "Chaining Periodic Three-Body Orbits in the EarthMoon System," *Acta Astronautica*, Vol. 67, 2010, pp. 623-638.
- [12] D. Folta, and T. Sweetser, "ARTEMIS Mission Overview: From Concept to Operations," AAS/AIAA Astrodynamics Specialist Conference, Girdwood, Alaska, July, 2011. Paper No. AAS 11-510.
- [13] V. Szebehely, *Theory of Orbits: The Restricted Problem of Three Bodies*, Academic Press, New York, United States, 1967.
- [14] T. Lam, and G. J. Whiffen, "Exploration of Distant Retrograde Orbits Around Europa," 15th AAS/AIAA Spaceflight Mechanics Meeting, Copper Mountain, Colorado, January, 2005. Paper No. AAS-05-110.
- [15] L. Capdevila, Purdue University, Private Communications, July 26, 2013.
- [16] J. Demeyer, and P. Gurfil, "Transfer to Distant Retrograde Orbits Using Manifold Theory," *Journal of Guidance, Control, and Dynamics*, Vol. 30, 2007. DOI: 10.2514/1.24960
- [17] C. J. Scott, "Transfer and Capture into Distant Retrograde Orbits," Ph.D. Thesis, Department of Aerospace Engineering, The Pennsylvania State University, University Park, Pennsylvania, May, 2010.
- [18] M. Vaquero, and K. C. Howell, "Leveraging Resonant Orbit Manifolds to Design Transfers Between Libration Point Orbits in Multi-Body Regimes," 23rd AAS/AIAA Space Flight Mechanics Meeting, Kauai, Hawaii, February, 2013. Paper No. AAS 13-334.
- [19] M. Vaquero, "Spacecraft Transfer Trajectory Design Exploiting Resonant Orbits in Multi-Body Environments," Ph.D. Thesis, School of Aeronautics and Astronautics, Purdue University, West Lafayette, Indiana, August, 2013.
- [20] A. F. Haapala, and K. C. Howell, "Representations of Higher-Dimensional Poincaré Maps with Application to Spacecraft Trajectory Design," IAF 63rd International Astronautical Congress, Naples, Italy, October, 2012. Paper No. IAC-12.C1.7.2.
- [21] C. C. Conley, "Low Energy Transit Orbits in the Restricted Three-Body Problem," *Society for Industrial and Applied Mathematics Journal on Applied Mathematics*, Vol. 16, 1968 pp. 732-746.
- [22] G. Gómez, W. S. Koon, M. W. Lo, and J. E. Marsden, "Connecting Orbits and Invariant Manifolds in the Spatial Restricted Three-Body Problem," *Nonlinearity*, Vol. 17, 2004, pp. 1571-1606.
- [23] M. Lara, and R. P. Russell, "On the Family 'g' of the Restricted Three-Body Problem," IX Jornadas de Trabajo en Mecánica Celeste, Jaca, Huesca, Spain, June, 2006.
- [24] M. Michalodimitrakis, "Hill's Problem: Families of Three-Dimensional Periodic Orbits (Part I)," *Astrophysics and Space Science*, Vol. 68, 1980. pp. 253-268.
- [25] R. A. Broucke, "Periodic Orbits in the Restricted Three-Body Problem with Earth-Moon Masses," NASA-JPL TR 32-1168, February, 1968.
- [26] D. Folta, T. Pavlak, A. Haapala, K. Howell, M. Woodard, "Earth-Moon Libration Stationkeeping: Theory, Modeling, and Operations," *Acta Astronautica*, February, 2013, DOI: <http://dx.doi.org/10.1016/j.actaastro.2013.01.022>.